Reaction mechanism of (α,d) transfer in ^{208}Pb$(\alpha,d)^{210}$Bi at 33 and 48 MeV

W. W. Daehnick, M. J. Spisak, and J. R. Comfort
Nuclear Physics Laboratory, University of Pittsburgh, Pittsburgh, Pennsylvania 15260
(Received 29 September 1980)

The reaction ^{208}Pb$(\alpha,d)^{210}$Bi has been studied at 33 and 48 MeV with particular emphasis on the $(h_{9/2}g_{9/2})$ ground-state multiplet and the high-spin members of other low-lying n-p multiplets, which are expected to be of high purity. About 50 angular distributions were obtained and used as a basis for a study of the transfer mechanism in (α,d) reactions. The analysis was made with the microscopic distorted-wave Born approximation and with two-step coupled-reaction-channel calculations. The L transfers observed ranged from $L=1$ to $L=13$ and were consistent with one-step transfer selection rules. Nevertheless, the relative magnitudes of cross sections to levels of the $(h_{9/2}g_{9/2})$ ground-state multiplet disagree with one-step-transfer predictions at either beam energy by factors which vary from 0.5 to 4.0. This phenomenon is explained as a coherent addition of the sequential stripping amplitudes $(\alpha,t;t,d)$ and $(\alpha,{}^3\text{He};{}^3\text{He},d)$ to the one-step amplitude, where the important $(\alpha,t;t,d)$ amplitude typically amounts to about 50% of the one-step (α,d) amplitude for high- and low-spin states alike. Details of the coupled-reaction-channel analysis are provided. The two-step calculations were kept free of arbitrary parameters by a simultaneous analysis of previously published ^{208}Pb(t,d), ^{208}Pb$({}^3\text{He},d)$, ^{208}Pb(α,t), and ^{208}Pb$(\alpha,{}^3\text{He})$ single-particle transfer data. This systematic reanalysis indicated again that most single-particle states in ^{209}Pb and ^{209}Bi show their full spectroscopic strength, but that the $\pi i_{13/2}$ and $\nu j_{15/2}$ single-particle states are not pure and have single-nucleon spectroscopic factors of about 0.75 ± 0.10.

[NUCLEAR REACTIONS ^{208}Pb$(\alpha,d)^{210}$Bi, $E_\alpha=33$ and 48 MeV, measured E_d and $\sigma(\theta,E_d)$ with QDDD spectrograph. DWBA and CRC analysis, deduced levels, $L_{\alpha,d}$, evidence for sequential stripping.]

I. INTRODUCTION

The special selection rules and form-factor sensitivities of two-particle transfer reactions[1] supplement single-nucleon transfers in an important way and have made them valuable tools in nuclear spectroscopy. However, the quantitative analysis of such processes has not yet reached the dependability of single-nucleon-transfer theories. For instance, the absolute normalization of (t,p) or (α,d) reactions is still based on empirical normalization factors[2,3] which are not fully explained by theoretical efforts (e.g., Ref. 4) and which, furthermore, tend to depend on the optical potentials used to generate the distorted waves. The motivation for the ^{208}Pb(α,d) study originally was to test and to calibrate the reaction (α,d) by studying a case where the initial ^{208}Pb ground state and at least ten of the final ^{210}Bi states are well known and simple. However, this simple test gave unexpected results. As we discuss below, it seems now that analyses of (α,d) reactions may have to become quite complex. It has been well documented that two-step processes in transfer reactions are important where one-step transitions are weak or forbidden.[5-10] There also is *theoretical* evidence that two-step processes should contribute significantly in direct allowed two-nucleon-transfer reactions[9,11,12]; however, until recently[13,14] little experimental evidence existed which convincingly demonstrated strong two-step contributions in direct allowed transitions.

II. EXPERIMENTAL PROCEDURES

The ^{208}Pb$(\alpha,d)^{210}$Bi experiment was carried out in two stages. The 33 MeV measurement was performed with the MP tandem of the Max-Planck Institut für Kernphysik in Heidelberg, Germany. The reaction deuterons were analyzed in the Heidelberg quadrupole-dipole-dipole-dipole (QDDD) spectrograph and detected by means of a 1.0 m long position-sensitive gas proportional counter[15] which simultaneously provided a ΔE signal for particle identification. After the initial counter calibration runs with α particles, deuteron identification was made simple by choosing an entrance foil for the focal plane detector thick enough (0.4 mm) to stop all α particles, but thin enough to cause only minor perturbations of the deuteron trajectories.

The intrinsic position resolution of the resistive-wire focal-plane detector at 45° incidence was about 1.5 mm and made a negligible contribution to the overall energy resolution. The spectrograph solid angle was $\Omega=9.97$ msr. The self-supporting >99% enriched ^{208}Pb target had a thick-

ness of 0.35 ± 0.12 mg/cm^2 as determined by the elastic scattering monitor, and it made the major contribution to the total experimental deuteron resolution of 16 keV. The stability of the target was monitored by measuring elastic α-particle scattering into a Si detector fixed near $\theta = 30°$. A typical (α,d) spectrum for the 33 MeV data is shown in Fig. 1. Data were taken in 10° steps over the range $10° \leq \theta \leq 60°$.

The ^{208}Pb(α,d) measurements at $E_\alpha = 48.2$ MeV were performed at the Princeton Cyclotron Laboratory. Ejectile detection again was accomplished with a 60 cm gas-filled position-sensitive proportional counter[16] in the focal plane of a QDDD spectrograph. At 48 MeV, elastic and inelastic α's do not interfere with deuterons of $E > 24$ MeV, and the two-dimensional array of position vs E signals, derived from a plastic scintillator behind the position detector, provided excellent deuteron identification. A new self-supporting ^{208}Pb target isotopically enriched to $\geq 99\%$ and with a thickness of 0.317 ± 0.020 mg/cm^2 was used. For this experiment the target thickness had been determined in advance by low-energy α scattering at the Pittsburgh tandem accelerator. A typical α beam of 0.3 μA was maintained throughout most runs, and target integrity was monitored by a NaI counter fixed at $\theta = 60°$. No target degradation was noted. Charge collection was handled by a water-filled Faraday cup which at small beam currents tended to show a 5–15% error in the charge integration; hence runs were normalized to the NaI monitor counts. Adding estimates for uncertainties in target thickness, charge integration, effective solid angle,

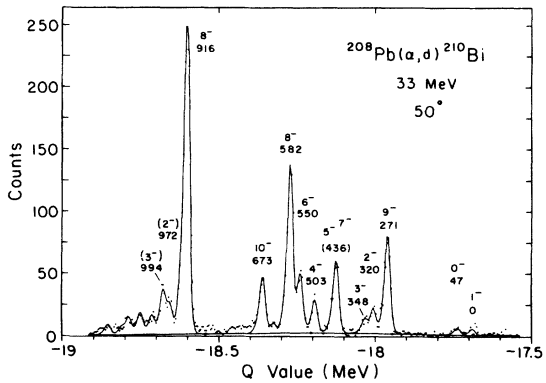

FIG. 1. Typical ^{208}Pb$(\alpha,d)^{210}$Bi spectrum as observed in a single run with the focal plane detector in the Heidelberg QDDD spectrograph at $E_\alpha = 33$ MeV. The ^{210}Bi excitation energies are given in keV. Spin assignments are from prior work. The solid lines show AUTOFIT least square fits to the peaks using a peak shape of standard shape and constant width in Q. The background was assumed smooth as shown.

and detector efficiency, we compute an absolute scale uncertainty in our 48 MeV data of about 20%. The scale error at 33 MeV was about 35% and arose primarily from the target thickness uncertainty.

Due to the large dispersion of QDDD spectrographs, the deuteron resolution, 16 keV at 33 MeV and 25 keV at 48 MeV, was not limited by the detection systems, but was determined by contributions from target thickness and beam quality. The spread of the analyzed cyclotron beam was compensated in part through dispersion matching. QDDD dispersion together with the limited length of the focal plane detectors and the negative Q value of the ^{208}Pb(α,d) reaction (−17.67 MeV) limited the energy bites to about 2 MeV for each magnetic field setting. At 48 MeV, 2–3 magnetic field settings were used in order to see states up to 4 MeV excitation in ^{210}Bi. Figure 2 shows a (composite) deuteron spectrum for $\theta_{lab} = 30°$ at an incident α energy of 48.2 MeV. The decision to take several overlapping spectra proved to be time consuming, but it permitted automatic cross checks on the accuracy of the monitoring system and it simplified the determination of excitation energies. The level energies quoted are estimated to be accurate to 0.2% of excitation energy ($E = \pm 0.002E^*$) for levels above $E^* = 1.0$ MeV. Energies for the well known levels below 1 MeV were taken from the literature and were used to calibrate the focal-plane detector. The 48 MeV data were taken in 5° steps from $\theta = 10°$ to 40°. Although not presented in this paper, additional (α,d) data were taken at the same time,[17] at identical magnet field settings, for ^{206}Pb and ^{204}Pb targets. These data greatly aided in the identification of impurity peaks and in the energy calibration.

All Pb(α,d) data were analyzed by hand *and* by the use of the peak fitting program AUTOFIT.[18] The latter proved superior for analyzing strong but poorly separated peaks and in obtaining good energy calibrations, but it tended to be more cumbersome if impurities and nonuniform background presented problems. The major impurities interfering with our spectra resulted from the ^{12}C$(\alpha,d)^{14}$N (3.95 MeV) and ^{16}O$(\alpha,d)^{18}$F ($5^+, 3^+$ states) transitions. The identification of these impurities was confirmed by "background" runs with a Formvar target.

III. EXPERIMENTAL RESULTS

The angular distributions extracted from the 33 and 48 MeV data are presented in Figs. 3–6, ordered according to excitation energy. The data in Figs. 3 and 4 are compared with empirical

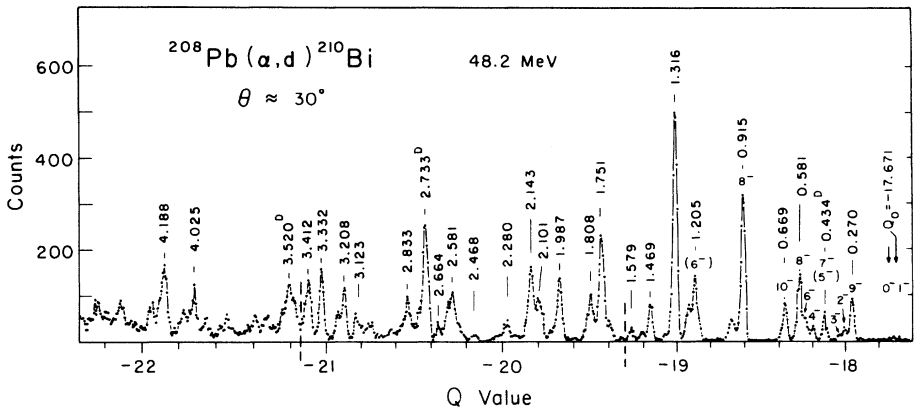

FIG. 2. Composite of three spectrograph spectra for ^{208}Pb(α,d) at 48.2 MeV. The raw data are replotted against Q value for the transitions. A normalized average of 25° and 35° spectra was substituted for small regions near $Q=-18$ and −19.8 MeV, which at 30° were obscured by broad ^{12}C(α,d) and ^{16}O(α,d) impurity peaks.

curves, and/or microscopic distorted-wave Born approximation (DWBA) and coupled-reaction-channel (CRC) calculations; in Figs. 5 and 6 the comparison is made with empirical curves derived from transitions to known final states. A systematic comparison of empirical, zero-range–DWBA and finite-range–DWBA curves[19] is shown in Fig. 7.

It is noted that a number of previously reported levels (e.g., at 563, 1194, 1338, 1382, 1464, 1476, 1923, and 1978 keV) are either not visibly excited or not resolved from stronger neighbors. Their weakness is attributed to low L-transfer values or to small spectroscopic amplitudes. The $\Delta T=0$ selection rule for (α,d) reactions which excludes population of 0^+ or $(j^2)_{J=\text{even}}$ states, cannot be tested directly in ^{210}Bi as no ΔT-forbidden states are known below 3.5 MeV. There is, however, good evidence in many lighter nuclei that this selection rule is obeyed in the absence of compound nuclear contributions in (α,d) and (d,α) reactions.[20,3,21]

As seen in Figs. 3 and 4 the presence of sequential stripping contributions does not substantially alter the basic L-dependent angular distributions, and to the extent that L_{transfer} can be established from relatively weakly structured angular distributions, our differential cross sections limit J^π of the new states to $L-1\leq J\leq L+1$, $\pi=(-1)^L$. We also observe certain other regularities: At 48 MeV "strong" $L=1$ transfers have typical peak cross sections of the order of 2 μb/sr, while $L=5$ transfers reach 20 μb/sr. $L=7$ and 9 transfers are most favored dynamically with $\sigma_{\text{peak}}\geq 100$ μb/sr, while $L=12$ and 13 are again suppressed somewhat and reach peak values of 30 μb/sr, in good agreement with microscopic DWBA predictions. This regularity can be used spectroscopically in the sense that the strong peaks cannot correspond to low-spin final states. For spectroscopic reasons the converse is not true in general.

Previously known (E^*,J^π) information[22-24] for ^{210}Bi is compared with our (α,d) results in Table I. Although energy measurements from ($d,p\gamma$) reactions have smaller uncertainties than our (α,d) values, the latter are nevertheless shown (as extracted from the peak-fitting procedure) since different final states are preferentially excited in the two reactions at higher excitation energies. Occasionally (e.g., for $E^*=435$ keV) the measured centroid of an unresolved doublet can be used to estimate the relative contributions of the two members. Most entries of Table I are self-explanatory, but it should be cautioned that L assignments from fitting (α,d) data may be uncertain by one unit for low L, and by two units for the highest L. Furthermore, there are no known $L=6$ and $L=8$ transitions. If L values are given without parentheses other available spectroscopic information has been used to limit the acceptable range of L.

We note that the number and spin sequence of the low-lying levels seen in the ^{209}Bi(d,p) studies[24] and in our ^{208}Pb(α,d) data correspond fairly well to the theoretical level schemes of Kim and Rasmussen,[25] Kuo and Herling,[26] or Ma and True.[27] Frequently, an approximate L determination will suffice to establish the correspondence between an experimental level and a limited number of theoretical states. A comparison of the three theoretical level schemes and our experimental one is shown in Fig. 8. Good overall agreement for the $(h_{9/2}g_{9/2})$ground-state multiplet is apparent. For the higher multiplets the calculations diverge. For instance, the 11^+

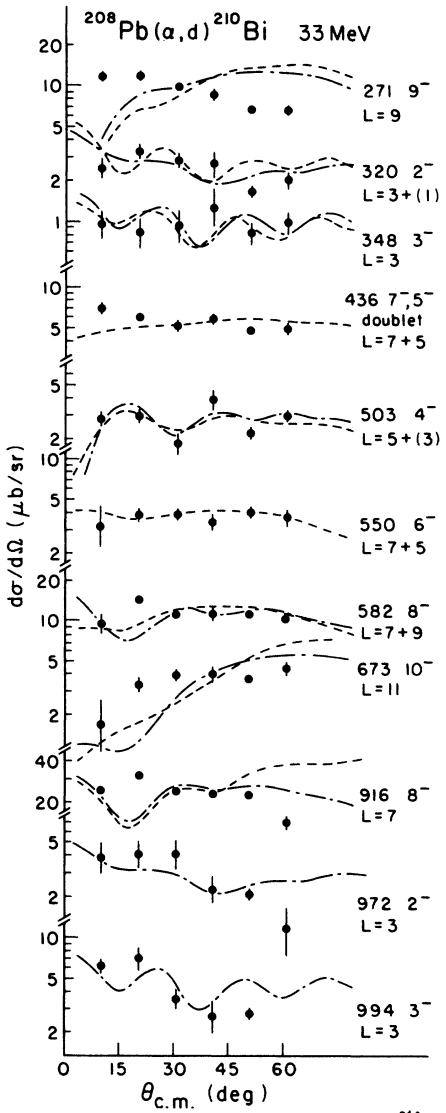

FIG. 3. Angular distributions to low-lying ^{210}Bi states, as observed in the 33 MeV experiment. Error bars include all random experimental errors, but not the overall scale uncertainty (35%). The dash-dotted lines represent microscopic (one-step) DWBA calculations. The dashed curves are second-order–DWBA calculations as explained in the text. The curves are independently normalized to the data.

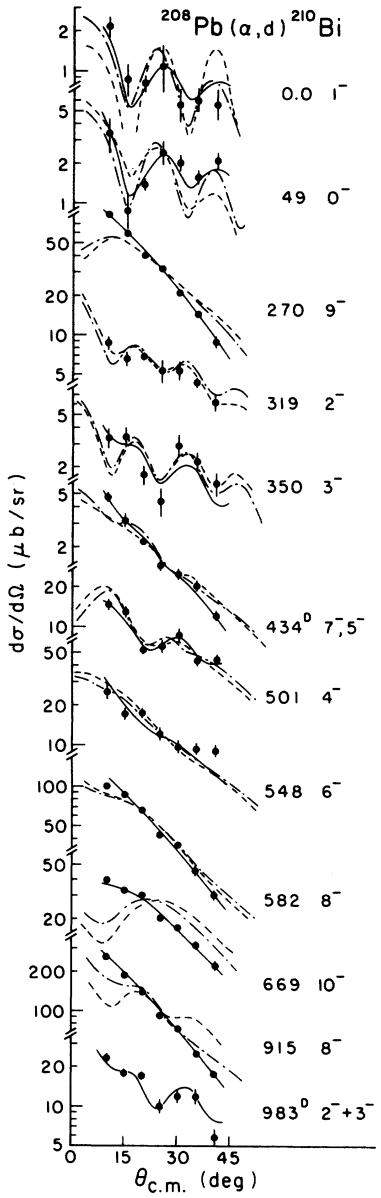

FIG. 4. The angular distributions for ^{208}Pb$(\alpha,d)^{210}$Bi at 48 MeV to known levels below 1 MeV are compared with empirical curves (solid lines) obtained from two or more known transitions of like L and two DWBA calculations which are normalized to the data. The dashed lines correspond to the second-order–DWBA calculations referred to in the text. The dash-dotted lines correspond to one-step microscopic DWBA calculations. We note that the CRC and the one-step DWBA curves are very similar to each other (and in reasonable agreement with the data) for transitions with $J^\pi \leq 7^-$, particularly for the enhanced cross sections (J^-_{even}). For $J \geq 8^-$ our zero-range DWBA curves begin to disagree with experiment. As explained in text the CRC curves are much superior to one-step DWBA in predicting the absolute cross sections; however, both calculations fail to reproduce the strong forward peaking observed experimentally.

state at 1.316 MeV which dominates the experimental (α,d) spectrum and should have the configuration $(i_{13/2}g_{9/2})$ is predicted by Kuo and Herling for 1.68 MeV and by Ma and True for 0.88 MeV. No such state at all is predicted by Kim and Rasmussen, who did not include the $i_{13/2}$ configuration in their model space. On the other hand, the $(h_{9/2}j_{15/2})_{12^+}$ level is found by all three calculations (and by experiment) near 1.5 ± 0.1 MeV. The strong 9^- state expected near 1.9 ± 0.2 MeV could not be identified with con-

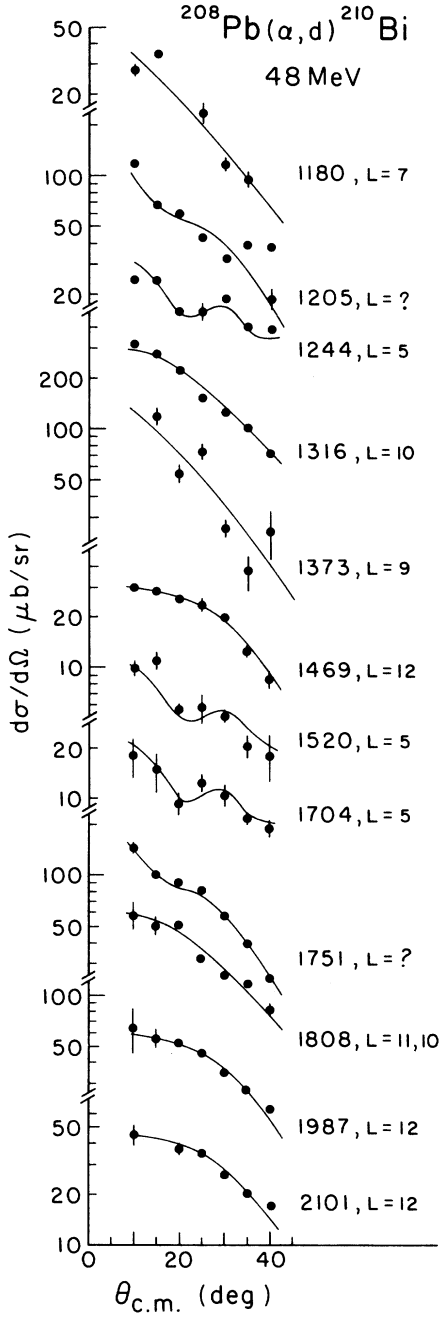

FIG. 5. 48 MeV angular distributions for $1.0 < E^* < 2$ MeV are compared with empirical curves in order to deduce values for the dominant L transfer. The L values shown identify the curve which best fit the data. Error bars are generally determined by uncertainties in the background subtraction. Peaks corresponding to the angular distributions are identified in Fig. 2. Level energies are given in keV.

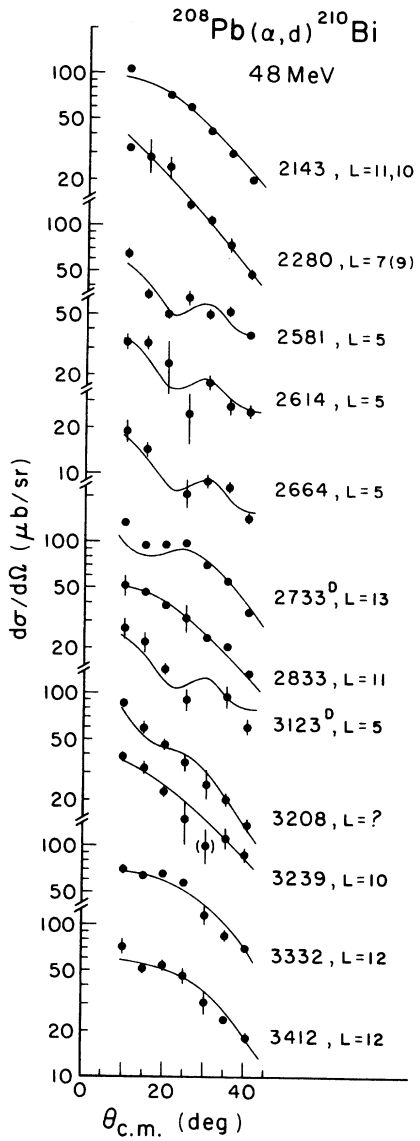

FIG. 6. 48 MeV angular distributions for $2.1 \leq E^* \leq 3.4$ MeV. See also caption for Fig. 5.

fidence in the (α, d) spectrum. One of the strong (α, d) levels in this range, all of which should have positive parity according to the (d,p) studies, may be an unresolved doublet. This $(f_{7/2} i_{11/2})_9$- level would not be seen in (d,p). The strong $(i_{13/2} j_{15/2})_{14}$- level (not shown in Fig. 8) is predicted by Kuo and Herling for 3.05 MeV and by Ma and True for 2.68 MeV. It is found experimentally at 2.733 MeV.[17]

IV. MICROSCOPIC DWBA CALCULATIONS

Given a closed shell target such as ^{208}Pb, and two-particle final-state wave functions for ^{210}Bi (from Ref. 26), microscopic two-nucleon transfer calculations[28] are relatively simple and have been performed with the zero-range DWBA code DWUCK4.[29] In calculations for the ^{208}Pb(α, d) reaction, the inclusion of the weak admixed con-

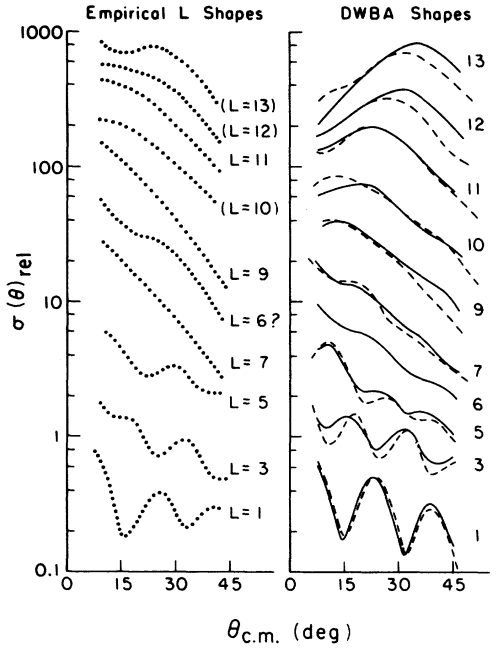

FIG. 7. Comparison of empirical Pb(α,d) angular distributions (dotted curves) used in Figs. 4–6 with one-step DWBA calculations for the range of L transfer encountered. The solid curves are finite-range calculations with cluster form factors (obtained with the potentials α_{III} and d_I of Table II, and assuming $E^*=1$ MeV). The dashed curves are microscopic DWBA calculations for particular states with known configurations and $0.5<E^*<2$ MeV. (The most recent curves are shown, which use potentials α_{II} and d_I.) We note that the finite-range curves here constitute a moderate improvement over zero-range, but do not bridge the gap to experiment which is evident for large L transfer. The finite-range curves generally have less structure than zero-range curves computed with the same parameters. We observed that ambiguities in the optical model parameters can produce changes in the computed angular distributions which are more pronounced than the effects of a finite range treatment.

figurations showed little effect on the predicted angular distributions. The comparison of the average empirical, finite-range cluster, and zero-range microscopic calculations shown in Fig. 7 for the range of angular momenta encountered shows a fairly good correspondence of empirical and DWBA curves for $L\leq 7$; but we find increasing differences, particularly at small angles, as L increases to $L=13$. It is for this reason that most comparisons between experiment and theory below are made in terms of the integrated cross sections, which are less sensitive to the behavior at extreme forward angles.

It is well known that seemingly secondary details of DWBA calculations can effect major changes in the results, particularly if the particle energies and the L transfer of interest involve poor "angular momentum matching." This is invariably the case if the L-transfer range is large. In this study $1\leq L\leq 13$, so that optical-potential, finite-range, and nonlocality effects are all quite noticeable. We make the equivalent of a first order finite-range correction by "matching" the potential wells (i.e., depths and geometry) when choosing optical model potentials.[3] While this procedure cannot equal a full finite range treatment, it gives a very reasonable first approximation (see Fig. 7). We do not use any *explicit* finite-range correction function. It has been found advisable to use nonlocality corrections for the scattered projectiles, and in this study we use the conventional zero-range nonlocality parameters,[29] i.e., $\beta_\alpha=0.2$, $\beta_d=0.54$, and $\beta_t=\beta_{^3He}=0.25$. The α-particle size factor used for the microscopic form factor is $a=1.52$ fm. As used in the DWUCK4 program this value produces a root-mean-square radius of 1.62 fm for the α particle. All other DWBA parameters are shown in Table II.

The single-nucleon binding energies for the two-nucleon transfer form factor were taken as $\frac{1}{2}$ (deuteron separation energy +2.225 MeV$+E^*$). The geometry of the potential well chosen for the n and p bound states in the two-particle-transfer reaction ($r_0=1.25$, $a_0=0.75$) is slightly larger than a conventional single-nucleon well. The resulting microscopic radial form factor corresponds closely to a deuteron cluster with corresponding quantum numbers in a well with $r_0=1.25$, $a_0=0.65$ (or $r_0=1.20$, $a_0=0.75$).

For single-nucleon transfers we prefer the bound state geometry $r_0=1.20$, $a_0=0.75$, over the two other commonly used sets ($r_0=1.25$, $a_0=0.65$) and ($r_0=1.2$, $a_0=0.65$). Our preferred geometry corresponds more closely to the real well for nucleon scattering above 20 MeV. Although the computed absolute cross sections differ little from the (1.25, 0.65) set, better fits to angular distributions are obtained.[24] We have found that the more diffuse bound-state well and a smaller value of the spin-orbit parameter ($\lambda=18$) produce correct spectroscopic factors over a wide range of l values. This assertion will be tested in Sec. V D for (t,d), $(^3He,d)$, (α,t), and $(\alpha,^3He)$ reactions on ^{208}Pb.

The optical potentials used for d, t, and ^3He scattering (Table II) are derived from systematic potentials[30,31] that fit a wide range of data. Furthermore, they have real well geometries that correspond closely to geometries resulting from target-projectile folding procedures and are preferred by us over others that give similar

TABLE I. Comparison of known properties of ^{210}Bi levels with results from the present work.

Previous work					Present (α,d) experiment (including Ref. 17)					
$E(NDS)$[a] (keV)	$E(d,p)$[b] (keV)	$E(d,p\gamma)$[c] (keV)	$l(d,p)$[b]	J^{π}[c]	$E(\alpha,d)$[d] (keV)	$\sigma_{33}(20°)$ (μb/sr)	$\sigma_{48}(10°)$ (μb/sr)	L	J^{π}	Dominant configuration
0	0	0	4	1^-	0	(1)	2.2	(1)	(1^-)	$\Pi h_{9/2}\nu g_{9/2}$
46.5	47	46	4	0^-	49	(2)	3.4	(1)	(0^-)	$\Pi h_{9/2}\nu g_{9/2}$
268	272	271	4	9^-	270	11.6	85	(9)	9^-	$\Pi h_{9/2}\nu g_{9/2}$
320	320	320	4	2^-	319	2.7	8.8	(3)	(2^-)	$\Pi h_{9/2}\nu g_{9/2}$
347	347	348	4	3^-	350	0.8	3.4	(3)	(3^-)	$\Pi h_{9/2}\nu g_{9/2}$
431	436[f]	433	4	7^-	435[f]	6.0	47	(7)	(7^-)	$\Pi h_{9/2}\nu g_{9/2}$
438		439	4	5^-					(5^-)	$\Pi h_{9/2}\nu g_{9/2}$
503	502	503	4	4^-	501	2.9	14.8	(5)	(4^-)	$\Pi h_{9/2}\nu g_{9/2}$
547	549	549	4	6^-	548	3.8	25	(5+7)	(6^-)	$\Pi h_{9/2}\nu g_{9/2}$
		563		(1^-)						
580	582	582	4	8^-	581	13.8	100	(7)	(8^-)	$\Pi h_{9/2}\nu g_{9/2}$
672	668	669	6	(10^-)	669	3.2	38	11	10^-	$h_{9/2}\nu i_{11/2}$
916	915	915	4	(8^-)	915	31.1	260	7	8^-	$f_{7/2}g_{9/2}$
966	971	972	2	(2^-)	972	3.4	23	(3)		
	993	993	6	(3^-)	994	4.4				
1172	1181[f]	1184	6	(8^-)	1180		35	(7-9)		$h_{9/2}i_{11/2}$
1202	1205	1209	(4,2)	(6^-)	1205		117	(6-9)		
1242	1247	1248	(4,2)	(4^-)	1244		24	(5)	(4^--6^-)	
1325	1317				1316		318	(10)	11^+	$i_{13/2}g_{9/2}$
	1336	1338	6	(6^-)	n.res.					$h_{9/2}i_{11/2}$
1372		1375	6	(3^-)	1373		(12)	($\leq$9)		$h_{9/2}i_{11/2}$
	1382[f]	1382		(7^-)						
1460		1464		(5^-)						
	1473[f]	1476	6,7	(9^-)	1469		30	(12)	(12^+)	$h_{9/2}j_{15/2}$
1517	1525	1525	(6)	(7^-)	1520		10	(5,6)		$(h_{9/2}i_{11/2})$
1577	1583	1584	2	(2^-)	1579		8.8			
(1706)	1705		(7)		1704		18.4	(5)		
(1738)	1750		7		1751		144			$h_{9/2}j_{15/2}$
(1778)	1775		7							
	1801		7		1808		58	(11,10)		$h_{9/2}j_{15/2}$
	1812		7							
(1835)	1835		7		1840		(28)			$h_{9/2}j_{15/2}$
					1908		(14)			
1916	1922	1923	2	(2^-)						$h_{9/2}d_{5/2}$
1972	1981[f]	1978	2	(7^-)						$h_{9/2}d_{5/2}$
		1988	2	(3^-)						$h_{9/2}d_{5/2}$
					1987		65	(12)	(11^+,12^+)	
2027	2033	2032	2	(5^-)	2034		(13.4)			$h_{9/2}d_{5/2}$
	2080	2080	2	(3^-)						$h_{9/2}d_{5/2}$
2102					2101		(44)	(12)		
	2107	2107	2	(6^-)						$h_{9/2}d_{5/2}$
2138	2143		2							
					2143		(107)	(11,10)		
2173	2176	2176	2	(4^-)	(2174)[e]		(20)			
2235	2236	2235	2	(6^-)	2231		(14)			
	2280		2		2280		(31)	(7,9)		
	2314									
	(2340)				2346		(9)			
	2464				2468		18			
2517	2523	2523	0	(4^-)	(2523)		(<10)			$h_{9/2}s_{1/2}$
					2543		19			
2572	2578	2577	0	(5^-)	2581		65	5	5^-	$h_{9/2}s_{1/2}$
2607	2611				2614		33	(5)		
					2664		19	(5)		
2727	2734	2734	(2+4)		2733[f]		134	(13)	(14^-)	$(i_{13/2}j_{15/2})$

TABLE I. (*Continued*).

Previous work					Present (α,d) experiment (including Ref. 17)					
$E(NDS)$[a] (keV)	$E(d,p)$[b] (keV)	$E(d,p\gamma)$[c] (keV)	$l(d,p)$[b]	J^{π}[c]	$E(\alpha,d)$[d] (keV)	$\sigma_{33}(15°)$ (μb/sr)	$\sigma_{48}(10°)$ (μb/sr)	L	J^{π}	Dominant configuration
2756	2762	2762	2							
					2773		(32)			
	2819		2+4							
2833					2833		52	(10,11)		
	2839	2838	(2+4)							
					2868		20.5			
2915	2920	2919	2		2924		23			
2960	2964	2963	(2+4)							
3007	3011	3008	(2+4)							
3033	3035	3035	(2+4)		3042		32			
3064	3067	3067	(2+4)							
					(3086)[e]		(15)			
3095	3102	3104	(2+4)							
					3123[f]		27	(5)		
3135	3138	3135	(2+4)							
3175	3180		2							
3205	3206		(2+4)		3208		88			
3228					3239		38	(10,11)		
	3242		(2+4)							
	3299									
	3330				3332		71	(12)		
					3412		73	(11,12)		
					3443		32			
					3502		66			
					3538		48			
					(4025)		(50)			
					(4188)		(70)			

[a] Reference 22.
[b] Reference 24.
[c] Reference 23.
[d] Excitation energies are uncertain to ±0.2%.
[e] Seen at only three angles.
[f] Doublet.

elastic fits as they permit improved DWBA results by potential-well "matching."[3]

The ^{3}He potentials of Ref. 31 had been derived from fits to targets with $A < 120$. When tested against data for 40 MeV ^{3}He scattering[32] from ^{197}Au it was found that the prescription of Ref. 31 overpredicted the imaginary depth W that was needed for a good fit by about 2.3 MeV. We slightly modified the isospin term in this prescription to $W = 41.7 - 0.33E + 32(N-Z)/A$ and obtained a very good Au(^{3}He,^{3}He) fit. The modified coefficient $32(N-Z)/A$ instead of $44(N-Z)/A$ was used for Table II.

The deuteron potentials $d_{\rm I}$ (prescription D in Ref. 30) were used for all calculations presented in this study. When the more general global potential prescription L became available,[30] potential set $d_{\rm II}$ was used for a number of cross checks. Only minor quantitative changes (<10%) were found and these could be offset by small changes in the DWBA normalization constants.

No systematic potentials were available for α particles near 48 MeV. The parameter sets $\alpha_{\rm I}$ and $\alpha_{\rm III}$ are extrapolations to 48 and 33 MeV, respectively, for a 25 MeV fit to ^{209}Bi.[3] Potential set $\alpha_{\rm II}$ was derived from a new fit to 58 MeV Pb(α,α) data presented in Ref. 33, under the conditions that r_0 and $r_{\rm I}$ be as close to 1.20 as possible while still maintaining a good elastic scattering fit and, furthermore, that the potential have a volume integral $J/4A \approx 350$ MeV fm^3. The $\alpha_{\rm II}$ potential produces better fits to the 58 MeV (α,α) data than set $\alpha_{\rm I}$, but it does not do quite as well for the (α,d) reactions. Since no potential was found that was excellent for both tasks, set $\alpha_{\rm II}$ was chosen for the 48 MeV analysis as being more appropriate in the framework of DWBA. A fit to the elastic scattering data of Ref. 33 is shown in Fig. 9.

The most extensive microscopic DWBA calculations were performed for the ten states of the $(h_{9/2}g_{9/2})$ ground state multiplet (Fig. 1). Ex-

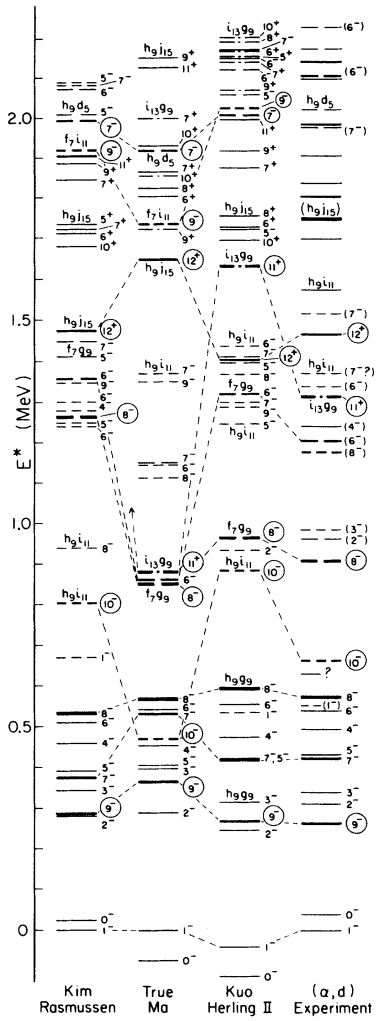

FIG. 8. Comparison of three large shell-model calculations for ^{210}Bi (Refs. 25–27) with levels seen in the (α, d) experiment and supplemental information on level spins from Refs. 17, 23, and 24. For $E > 1$ MeV only levels with $J \geq 5$ are shown, as (α, d) transitions to levels with spin < 5 are very weak. Levels which are seen with (α, d) cross sections in excess of 90 μb/sr, or are expected to have such strengths on the basis of their wave function, are drawn as heavy bars. Cross sections, seen or expected to be seen, with a strength of 30–90 μb/sr are shown by moderately heavy lines. The dominant configurations of the levels are distinguished by varied patterns for the horizontal bars: solid, double dash, triple dash, and dash-dot-dash. J_{max} states have their spin marked by a circle. Some of the levels expected to be seen strongly in (α, d) reactions have been correlated to the data by thin connecting lines. The zero energy point for the calculations is adjusted arbitrarily in order to get a good match for the ground state multiplet.

periments[23,24] and shell-model calculations alike[25-27] have suggested that at least nine of these ten states have dominant $(h_{9/2}g_{9/2})$ terms with amplitudes in excess of 0.98. (Reference 24 suggests that the purity of the 8^- state may only be 0.90.) Our initial microscopic DWBA calculation assumed a 100% pure $(h_{9/2}g_{9/2})$ ground state multiplet. This led to cross sections for several multiplet members in disagreement with experiment by an order of magnitude [if the zero-range (α, d) calculations were normalized to the strong 9^- state.] In a second calculation the complete ^{210}Bi wave functions of Kuo and Herling[26] (approximation II) were used. This led to roughly a factor of 1.7 enhancement in the predictions for most of the $(h_{9/2}g_{9/2})$ states. A notable exception is the 9^- transition, which was increased by only 1.1. This refinement constitutes a noticeable improvement, but does not begin to overcome the systematic failure encountered. Figure 10 graphically represents the absolute normalization factors for zero-range DWBA, which are needed to match the microscopic calculations to the 33 and 48 MeV cross sections of Figs. 3 and 4, and to the four strongest J_{max} states at higher excitation. For the $(h_{9/2}g_{9/2})$ states the disagreements show an interesting regularity: All natural parity states of the multiplet are *overpredicted* by DWBA (relative to the average normalization of 4800) and need renormalizations of about a factor of $\frac{1}{2}$. On the other hand, the cross sections for unnatural parity states (0^-, 2^-, 4^-, 6^-, 8^-) are *underpredicted* by factors of from 1.5 to 4 and, as a group, would require renormalization by a factor of about 2. The other levels included in Fig. 10 are the pure $(h_{9/2}i_{11/2})_{10^-}$ level at 0.669 MeV, the $(f_{7/2}g_{9/2})_{8^-}$ level at 0.915 MeV, the $(i_{13/2}g_{9/2})_{11^+}$ level at 1.316 MeV, the $(h_{9/2}j_{15/2})_{12^+}$ level at 1.469 MeV, and the $(i_{13/2}j_{15/2})_{14^-}$ level at 2.733 MeV. Several of these J_{max} levels have unnatural parity, but all are *overpredicted* by DWBA. It was found by further calculations that the use of ^{210}Bi wave functions from Refs. 25 and 27 does not improve this picture. With the possible exception of the two 8^- states,[23,24] there is no current evidence that the wave functions of these selected ^{210}Bi states are much more strongly mixed than predicted by Ref. 26. Hence it seems proper to suggest that the deficiencies observed have their cause in our oversimplified assumptions about the reaction mechanism.

V. CONTRIBUTIONS FROM SEQUENTIAL STRIPPING PROCESSES

A. General considerations

As is evident from Fig. 10 the strongly oscillating normalization factors N for neighboring

TABLE II. Optical model parameters used in the $^{208}(\alpha,d)$ study. The parameter sets d_I, t, and ^{3}He belong to global, energy-dependent prescriptions. The energies appropriate for the various DWBA calculations are listed.

Projectile	E_{Lab} (MeV)	V_o (MeV)	r_o (fm)	a_o (fm)	r_c (fm)	W_V (MeV)	$4W_D$ (MeV)	r_I (fm)	a_I (fm)	V_{so} (MeV)	r_{so} (fm)	a_{so} (fm)	Reference
α_{I}	48	182.8	1.20	0.75	1.40	24.2	0	1.40	0.60	0			3 (^{209}Bi fit), adjusted for $E=48$
α_{II}	48	169.0	1.26	0.715	1.40	37.57	0	1.26	0.82	0			33 ^{208}Pb fit
α_{III}	33	194.4	1.20	0.75	1.4	21.9	0	1.40	0.60	0			3 (^{209}Bi fit)
d_{I}	41.8	86.7	1.20	0.75	1.3	1.150	50.78	1.31	0.89				
d_{I}	29	89.35	1.20	0.75	1.3	0.552	54.01	1.31	0.89				30 (pot. *C*)
d_{II}	29	93.14	1.17	0.759	1.3	1.074	47.56	1.325	0.915	6.48	1.07	0.66	30 (pot. *L*)
d_{I}	14	92.0	1.20	0.75	1.3	0	57.73	1.31	0.89				30 (pot. *C*)
t	31.5	158.33	1.20	0.72	1.3	12.95		1.40	0.84				31
t	25.6	159.33	1.20	0.72	1.3	14.92		1.40	0.84				31
t	20.0	160.23	1.20	0.72	1.3	16.77		1.40	0.84				31
t	16.5	160.83	1.20	0.72	1.3	17.93		1.40	0.84				31
^{3}He	44.2	154.96	1.20	0.72	1.3	33.88		1.40	0.88				31
^{3}He	40.8	155.9	1.20	0.72	1.3	35.39		1.40	0.88				31
^{3}He	30.9	157.4	1.20	0.72	1.3	38.38		1.40	0.88				31
^{3}He	16.0	159.93	1.20	0.72	1.3	43.30		1.40	0.88				31
bound p		a	1.20	0.75	1.3					$\lambda=18$			single nucleon
bound n		a	1.20	0.75	1.3					$\lambda=18$			transfer
bound n,p		a	1.25	0.75	1.3					$\lambda=20$			two-nucleon transfer

[a] Well depth adjusted by code to fit separation energy.

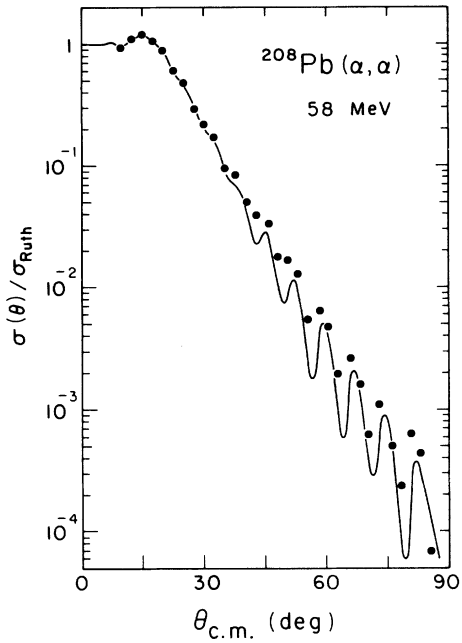

FIG. 9. Fit to the ^{208}Pb(α,α) elastic scattering data at 58 MeV by potential set α_{II}. [Several α potentials that would give better fits at large angles exist; however, these parameter sets produce serious problems with (α,t)-transfer cross sections.]

states of the ($h_{9/2}g_{9/2}$) multiplet are very similar at 48 and 33 MeV. They are primarily sensitive to whether J is odd or even rather than to the L transfer; e.g., N values for the 2^- and 3^- states differ greatly, but both transfers go by $L=3$. It seems most unlikely that inadequate optical-model parameters could artificially produce such a J- but not L-dependent effect or that these oscillations might find their explanation in a full finite range treatment of the reaction dynamics. Rather, the data suggest that two different processes of comparable strength contribute to the population of the final states and, depending on the J transfer, interfere constructively or destructively. Since the first excited state of ^{208}Pb lies at 2.61 MeV (i.e., ≥ 2 MeV above the multiplet) and is only weakly collective ($\beta=0.1$), the two-step contribution from inelastic scattering followed by np transfer is expected to be very small. However, successive transfer of the type ($\alpha,t;t,d$) or ($\alpha,{}^3$He;^{3}He,d) is a distinct possibility and relatively easy to calculate in second order Born approximation. As we reported previously,[14] calculations that incorporate both direct and successive-stripping amplitudes do indeed give a qualitatively correct account of the observed transition strengths. We shall concentrate in this section on the details of the construction of such two-step amplitudes.

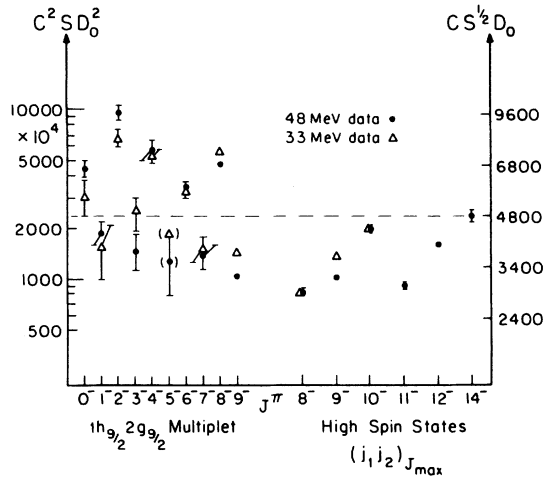

FIG. 10. Plot of empirical zero-range DWBA normalizations $N=C^2SD_0^2$ (MeV^{2}fm^3). The points are obtained by dividing integrated experimental cross sections for known states by microscopic predictions. The ratios N are plotted against the J^π values of the calibration states. N should be constant to the extent that the low-lying ^{210}Bi levels are well predicted by the shell model calculation of Ref. 26, provided that one-step microscopic DWBA is a useful description of the (α,d) reaction mechanism. We observe $900\times10^4<N<9000\times10^4$ and note that some of the largest jumps occur for adjacent J values. It is argued below that this large spread and the strong J dependence of N are primarily due to the neglect of sequential stripping contributions. This graph also suggests the possibility of a mild L dependence of N. It suggests no significant energy dependence. Note that the 33 MeV ratios (triangles) and the 48 MeV ratios (dots) agree to almost within the experimental uncertainties. The dashed line indicates the one-step (α,d) normalization chosen for the CRC calculations.

B. The model space

In principle, the interaction of α particles with a nucleus is very complex, and a full description of the reaction dynamics would need to be done in the CRC formalism.[34,35] In this framework the homogeneous Schrödinger equation is replaced with a set of coupled inhomogeneous equations

$$\left\{\frac{d^2}{dr_\alpha^2}-\frac{l_\alpha(l_\alpha+1)}{r_\alpha^2}+\left[k_\alpha^2-\frac{2\mu_\alpha}{\hbar^2}U_\alpha(r_\alpha)\right]\right\}\chi^J_{l_\alpha j_\alpha}(k_\alpha,r_d)$$

$$=\sum_\beta\frac{2\mu_\alpha}{\hbar^2}V_{\alpha\beta}\chi^J_{l_\beta j_\beta}(k_\beta,r_\beta)\,, \quad (1)$$

where the χ^J_{lj} are expansion functions of the total wave function of the system with total angular momentum J into channel wave functions

$$\psi^\alpha_{JM}=\{[i^{l_\alpha}Y_{l_\alpha}\otimes\phi_{s_\alpha}]_{j_\alpha}\otimes\Phi_{I_\alpha}\}_{JM}. \quad (2)$$

The intrinsic wave functions of the projectile and target are ϕ_{s_α} and Φ_{I_α}, respectively, and they

have relative orbital angular momentum l_α. The square brackets in Eq. (2) denote vector coupling. The off-diagonal coupling potentials $V_{\alpha\beta}$ are usually calculated from standard models in the zero-range approximation.[35-37,29] Corrections due to the nonorthogonality of the channel wave functions are neglected in Eq. (1).

In order to make calculations manageable, the complexity implicit in the use of Eq. (1) must be considerably reduced. Fortunately, the relatively simple shell-model nature of ^{208}Pb and its neighbors (see Fig. 11) greatly aids in this respect, as many of the truncations can be physically justified. Since cross sections for single-nucleon-transfer reactions on ^{208}Pb are one to two orders of magnitude larger than the (α,d) cross sections, two-step contributions from successive nucleon transfer could easily be important. On the other hand, as mentioned in Sec. V A, inelastic excitations are only weakly collective, so that multistep contributions that include these processes can be expected to be relatively small.

The set of two-step paths, now consisting of $(\alpha,t;t,d)$ and $(\alpha,{}^3\mathrm{He};{}^3\mathrm{He},d)$ processes (Fig. 12), can be restricted further by considerations of the ^{210}Bi wave functions. In all of the theoretical models[25-27] most of the low-lying states have relatively pure shell-model configurations. The amplitudes of the admixtures are typically of the order of 0.1 or less. Consequently, we consider as intermediate states in the mass-209 nuclei only those single-particle states that correspond to the dominant term of the final ^{210}Bi wave function for the state of interest. For example, in the two-step contributions to the $(h_{9/2}g_{9/2})$ multiplet of ^{210}Bi, we assume that the $(\alpha,t;t,d)$ reaction proceeds only through the $\frac{9}{2}^-$ ground state of ^{209}Bi, while the $(\alpha,{}^3\mathrm{He};{}^3\mathrm{He},d)$ reaction proceeds only through the $\frac{9}{2}^+$ ground state of ^{209}Pb. We find that the calculated two-step cross sections tend to be smaller than the one-step cross sections by factors of 3–10. Therefore it seems justifiable to include the full description of the ^{210}Bi wave functions in the calculation of the one-step amplitudes but to ignore all except the dominant term for the two-step processes.

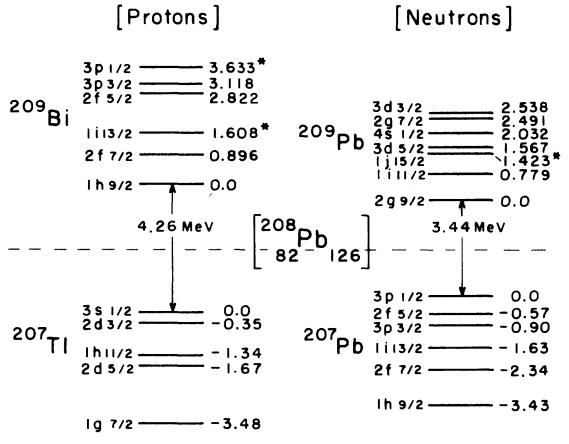

FIG. 11. Single particle and hole orbitals and experimental energies in the region of the double shell closure for ^{208}Pb. The calculations of Refs. 26 and 27 include all configurations based on the orbits shown above the closed shells. An asterisk behind the single particle energies indicates that the level is not a pure single particle state and contains significantly less than the full spectroscopic strength.

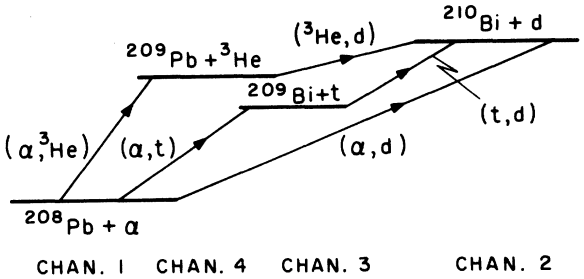

FIG. 12. Definition of the one-way-coupled CRC channels used in our "second-order DWBA" calculations. The nuclei ^{208}Pb, ^{209}Pb, and ^{209}Bi are all assumed to be in their ground states for the transfers to the $(h_{9/2}g_{9/2})$ multiplet in ^{210}Bi. The ^{209}Pb and ^{209}Bi nuclei are assumed to be in excited but pure single-particle states for transitions to the higher-lying $J_{\max}$ states.

Finally, the full CRC structure of Eq. (1) is not used. Instead, we consider only the forward-going reactions and ignore the couplings between the $t+{}^{209}$Bi and ^{3}He $+{}^{209}$Pb channels. This implies that $V_{\alpha\beta}=0$ for those channel couplings corresponding to pickup processes. It also eliminates three-step contributions to the ^{210}Bi states. Hence the two-step calculations are carried out in second-order DWBA. The computations reported here were made with the zero-range CRC program CHUCK3 operating in this mode.[38] Due to the large computational requirements for some of the transfer amplitudes, the one-step and the individual two-step amplitudes were computed separately, saved on disk files, and combined later with the program SUMAMP.[39]

C. Spectroscopic amplitudes and phases

The $V_{\alpha\beta}$ coupling matrix elements in Eq. (1) contain products of spectroscopic amplitudes for particle transfers between projectile states and between target states. These could be evaluated in either the pn representation or the isospin representation. However, for consistent

and proper normalizations in the CHUCK3 program, especially for the one-step (α,d) reaction, the isospin representation must be used. The relevant quantities in this case are $CS^{1/2}$ where C is the usual isospin Clebsch-Gordan coefficient.

The spectroscopic amplitudes for each of the one-step and two-step paths are easily evaluated in the case that ^{208}Pb is taken to be a doubly closed-shell nucleus. Every one-nucleon-transfer amplitude has[40,41] $|CS^{1/2}|=1$; the direct (α,d) path has $|CS^{1/2}|=1/\sqrt{2}$, since the two nucleons are always transferred to different orbitals.[1] In practice, the single-nucleon-transfer amplitudes $D_0CS^{1/2}$ were determined by the data for such reactions on ^{208}Pb (see Sec. V D) and the (α,d) amplitudes were multiplied by the coefficients of the corresponding terms of the ^{210}Bi wave functions.

The phases associated with the amplitudes are of great importance. The CHUCK3 program uses single-particle wave functions that are positive at large radii and associates i^l factors with all spherical harmonics. The shell-model wave functions[25-27] used different phase conventions for these items and some input adjustments were therefore necessary, the i^l factors being significant only for the configuration-mixed amplitudes of the direct (α,d) path. Additional phase factors are obtained from considerations of the role of antisymmetry in the rearrangements of fermions between initial and final states.[42]

The channel wave functions specified in Eq. (2) must be fully antisymmetrized among all nucleons. One can express them, for example, as the product of creation operators of two sets, a set for the projectile and a set for the target. A definite ordering is assumed, with the projectile particles appearing before the target particles and with a sequential numbering of particles imposed. Furthermore, the shell-model states of the target are also taken to be in some definite order; the projectile has only $s_{1/2}$ particles in its own system. Channel wave functions are then written for initial and final channels α and β. Transfer reactions will produce some interchanges between the projectile and target sets, and one must identify the rearrangements under a consistent set of procedures. Interchanging two particles (or a particle and a group) will introduce a phase factor $(-1)^{j_1+j_2-j'}$ for angular momentum and a phase $(-1)^{t_1+t_2-t'}$ for isospin, where j' and t' are the intermediate couplings of particles (groups) 1 and 2. An odd permutation of the particle numbering sequence will result in an additional factor of -1 since the particles are fermions.

These rearrangement phases are not contained in CHUCK3 but must be incorporated with the spectroscopic amplitudes. Table III summarizes the amplitudes and reordering phases that must be supplied in the program data deck for CHUCK3. Phases from the bound-state tails and i^l factors are additional. The angular-momentum phase factor for the $(\alpha,t;t,d)$ path arises because the j_2 neutron of the second step must be reordered across the j_1 proton of the first step. The phases in Table III differ slightly from those published earlier (Ref. 14). This situation arises from some changes in phase conventions between the CHUCK2 and CHUCK3 programs, as well as corrections of some inconsistencies in CHUCK2. The results of the calculations are the same in both cases. The validity of the phase evaluations is supported by test cases where the results are known from independent symmetry considerations.

D. Optical model potentials

The diagonal optical potentials $U_\alpha(r_\alpha)$ in Eq. (1) are usually chosen to reproduce elastic-scattering data. Such a requirement is most evident if the full CRC apparatus (including nonorthogonality corrections) is used with a large model space. It is, however, difficult to obtain the proper optical potentials in the full CRC environment, since the back-coupling amplitudes to each channel would invalidate the use of conventional optical-model search codes that operate in a single-channel approximation. Calculations of this magnitude are beyond the scope of the present study.

The truncations of the model space of the calculations, as discussed in Sec. V B, were intended to make the calculations more tractable, but they also introduce a number of ambiguities. Since the optical potential is an effective interaction that already simulates many of the effects of couplings to other reaction channels, it can be hoped that the neglect of the back-coupling

TABLE III. Spectroscopic amplitudes and reordering phases required for the calculation of the direct (α,d) and two-step paths in program CHUCK3. A ^{208}Pb target and pure shell-model configuration are assumed. The transferred particles have total angular momenta j_1 and j_2, and J is the total angular momentum of the final state in ^{210}Bi.

Channel	Phase $\times(CS^{1/2}D_0)_1\times(CS^{1/2}D_0)_2$			
(α,d)		4800		$j_1\neq j_2$
$(\alpha,t;t,d)$	$(-1)^{j_1+j_2-J}$	(−735)	(−226)	
$(\alpha,{}^3\mathrm{He})({}^3\mathrm{He},d)$	−1	(+707)	(−237)	

amplitudes in the present calculations is not a serious defect. Studies of proton scattering from ^{12}C have indicated that a one-channel optical potential can simulate many of the effects of a larger CRC environment.[43] We assume this result to be true in the present case as well, at least for the alpha and deuteron channels. The selection of the optical-model potentials for these channels was discussed in Sec. IV.

A much more serious uncertainty exists for the mass-3 optical potentials used for the intermediate channels. It is customary to generate the distorted waves for intermediate-state projectiles from the same optical potentials as for free projectiles at the same center-of-mass energy. However, this procedure is known to give serious errors in certain CRC and two-step calculations, particularly when deuteron intermediate channels are involved.[44,45] Folded potentials generally give better results. It is believed that the difficulty is closely associated with the breakup spectrum of the composite projectile. Since the energies of nucleon binding in the alpha particle or mass-3 projectiles are larger than for the deuteron system, the effects of breakup are not expected to be as large.[45]

Within the conventional framework, therefore, we proceeded to select optical potentials that gave good agreement with elastic-scattering data as well as good agreement with data for single-nucleon-transfer reactions on ^{208}Pb as computed in DWBA. At the same time we obtained values for the zero-range normalization constants required for each step of the two-step paths. These normalization constants are at times quite sensitive to the optical potentials selected.

The ^3He and t potentials and the bound nucleon potentials used for our calculations are given in Table II. Comparisons of DWBA calculations with data for the $^{208}Pb(\alpha,^3He)^{209}Pb$ reaction at 58 MeV,[33] the $^{208}Pb(\alpha,t)^{209}Bi$ reaction at 42 MeV,[46] the $^{208}Pb(^3He,d)^{209}Bi$ reaction at 44.2 MeV,[47] and the $^{208}Pb(t,d)^{209}Pb$ reaction at 20 MeV (Ref. 48) are shown in Figs. 13–16. The agreement with the data is generally very good except for some persistent difficulties with the (α,t) reaction. Finite-range effects may be significant in this case.

The best average normalization amplitudes $C\mathcal{S}^{1/2}D_0$ for each reaction extracted from the comparisons of Figs. 13–16 are given in Table III. They are in good agreement with expectations[38] for all branches. Transitions to single-particle states for all reactions shown were found to be consistent with $\mathcal{S}=1$ with the following exceptions: population of the $j_{15/2}$ level at 1.426 MeV in ^{209}Pb yielded $\mathcal{S}=0.70$ in the $(\alpha,^3He)$ analysis and 0.80 in the (t,d) analysis; population of the $i_{13/2}$ level at 1.608 MeV in ^{209}Bi yielded $\mathcal{S}=0.9$ (±0.3) in the (α,t) analysis and $\mathcal{S}=0.63(\pm0.1)$ in the $(^3He,d)$ analysis. The values are in general agreement with previous analyses.[33,46-49] The (α,d) normalization of 4800 was chosen from the best *average* fit in the one-step analysis.

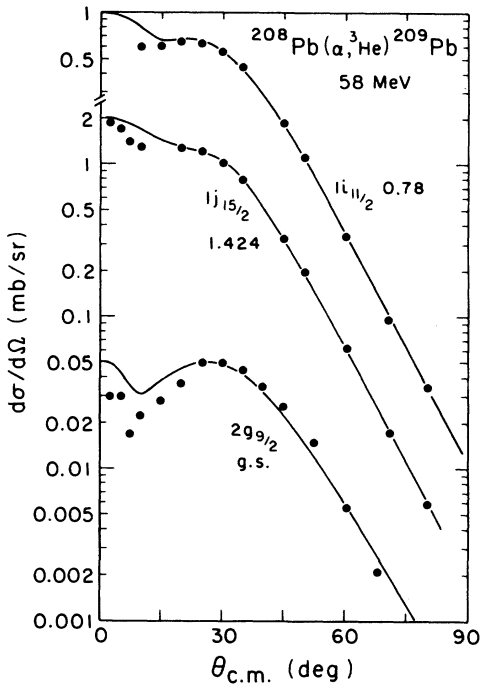

FIG. 13. DWBA analysis of the 58 MeV $^{208}Pb(\alpha,^3He)^{209}Pb$ data of Ref. 33 with the "systematic" parameter sets $(\alpha_{II},d_I,t,^3He)$ of Table II. The DWBA curves assume spectroscopic factors of $\mathcal{S}=1$, except for the $j_{15/2}$ transition where $\mathcal{S}=0.70$ was used. The zero-range DWBA normalization extracted is $C\mathcal{S}^{1/2}D_0=707\pm20$.

With the mass-3 optical potentials in Table II, we found that the $^{208}Pb(\alpha,t;t,d)^{210}Bi$ cross sections were about 20 times larger than those for the $^{208}Pb(\alpha,^3He;^3He,d)^{210}Bi$ channel. Apart from Coulomb effects, the two paths should be comparable in most every aspect. A large reduction in the ^3He channel is produced by its very much deeper imaginary optical potential term. It is not obvious to us that such a large difference has much physical significance. We point to this large ratio as one aspect that may need further study.

E. Results of sequential stripping calculations

To show a typical result, Fig. 17(a) presents the partial and the summed differential cross sections for the population of the $(h_{9/2}g_{9/2})_4^-$ state. Experimentally, this state is of intermediate strength (10 μb) and enhanced by a fac-

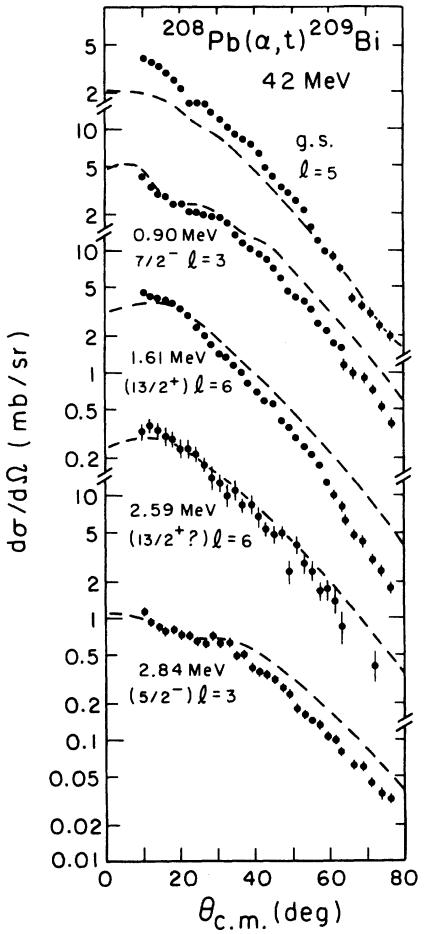

FIG. 14. DWBA analysis of the 42 MeV ^{208}Pb(α,t)^{209}Bi angular distributions of Ref. 46 with the systematic parameters of Table II. Compared to the original study the fits are moderately poor. This may be a consequence of requiring that (α_{II}) the α potential used must fit the Pb(α, α) scattering at 58 MeV. No α potential was found that gave a good fit to both the (α, α) and the (α, t) data. The DWBA curves were computed with the assumption that the spectroscopic factors are unity, except for the $l=6$ curves for which we assumed $S_1=0.9$ and $S_2=0.09$, respectively. As shown, the curves have the zero-range normalization $CS^{1/2}D_0=735\pm70$. A typical value for this normalization is 680 (Ref. 38).

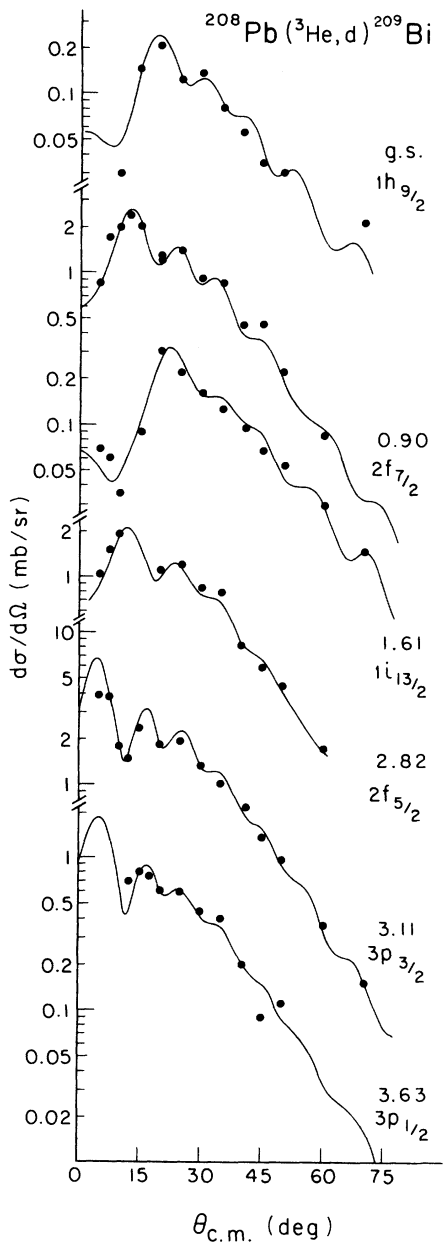

FIG. 15. DWBA analysis of the ^{208}Pb(^{3}He, d)^{209}Bi proton-transfer at $E_{^3He}=44.2$ MeV. The data of Ref. 47 are compared with DWBA calculations using the systematic parameter sets of Table II. The fits are of a quality very similar to the original study; the $i_{13/2}$ fit is somewhat improved. The zero-range normalization for the DWBA curves is $CS^{1/2}D_0=237\pm10$. We assumed $S_j=1$ for the $h_{9/2}$, $f_{7/2}$, $f_{5/2}$, and $p_{3/2}$ states. A spectroscopic factor $S=0.63$ is deduced for the $i_{13/2}$ transition and $S=0.35$ is extracted for the $p_{1/2}$ transfer. It can be seen that the fit for the $p_{3/2}$ transfer would also be improved somewhat if a spectroscopic factor smaller than 1.0 were used.

tor of about 2.5 over a typical one-step (α, d) prediction. As seen in Fig. 17(a) the one-step partial cross section (computed with its full microscopic form factor) remains the largest individual contribution. The next largest partial cross section comes from the two-step process (α, t; t, d). The smallest contribution arises from (α, ^{3}He; ^{3}He, d). We note that the interference between the two two-step channels (labeled AT and AH) is constructive, a feature that is seen for all ($h_{9/2}g_{9/2}$) levels. Finally, the coherent

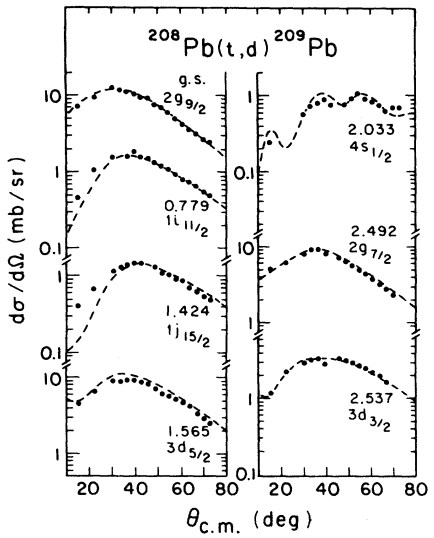

FIG. 16. DWBA analysis of the ^{208}Pb$(t,d)^{209}$Pb reaction at 20 MeV with the systematic parameter sets of Table II. The data are from Ref. 48. All spectroscopic factors were entered as 1.0, except for the $1j_{15/2}$ transition where $S=0.8$ was used. The zero-range DWBA normalization extracted was $CS^{1/2}D_0=226\pm10$. (Fits to the $d_{5/2}$ and $s_{1/2}$ states would be improved if $S<1$ were used.)

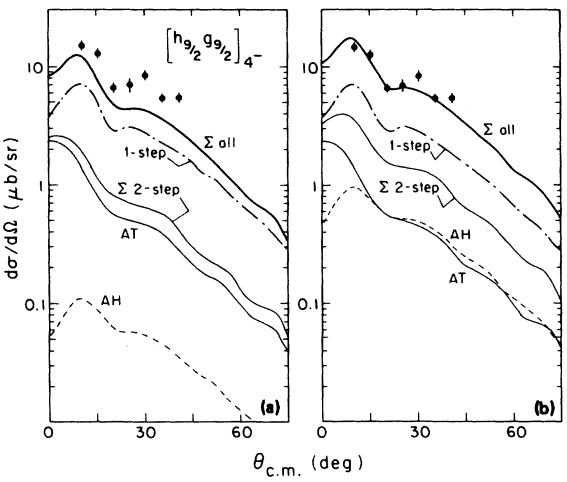

FIG. 17. Comparison of our second-order DWBA calculations with the experimental angular distribution for the $(h_{9/2}g_{9/2})_{4^-}$ state. (a) The calculation with no adjustable parameters is shown. The solid line represents the full second-order–DWBA cross section. Curve AT presents the cross section for the $(\alpha,t;t,d)$ two-step reaction. Curve AH correspondingly refers to the $(\alpha,{}^3\mathrm{He};{}^3\mathrm{He},d)$ sequential stripping transfer. Although the sum of the two-step transfers amounts to only about 30% of the one-step cross section, it is seen that the coherent sum of all channels results in an 80% increase over the one-step value. The final angular distribution is not significantly different from that for the one-step calculation. (b) The influence of the $(\alpha,{}^3\mathrm{He};{}^3\mathrm{He},d)$ channel by enhancing the computed $(\alpha,{}^3\mathrm{He};{}^3\mathrm{He},d)$ amplitude until it becomes comparable to the $(\alpha,t;t,d)$ path is shown. (The AH amplitude was multiplied by 3.0; no other changes were made.) In this case the coherent two-step cross section grows to about 50% of the one-step value, and the coherent sum of all contributions reaches a value 2.5 times that of the one-step transfer, which is close to the experimentally observed cross sections. The empirically needed enhancement of the two-step contribution may have a physical justification: It has been found theoretically for (p,t) reactions that the two-step amplitude is increased if account is taken of the virtual breakup states for the intermediate projectile (Ref. 53).

sum over all three channels yields a cross section 1.7 times larger than the one-step channel alone. The summed cross section differs from the one-step angular distribution primarily in scale and not in shape. For the adjacent 5^- level the results are similar for the partial cross sections, but when all three channels are added coherently the sum is *smaller* than the one-step cross section.

For all members of the $(h_{9/2}g_{9/2})$ multiplet the coherent effects depend on J being even or odd. This results in a staggered pattern of the integrated cross sections.[14]

It is of interest to note that the channel $(\alpha,{}^3\mathrm{He};{}^3\mathrm{He},d)$, labeled AH in Fig. 17, enhances this staggered effect noticeably if its amplitude is increased. Figure 17(b) illustrates a situation for the $(h_{9/2}g_{9/2})$ states which comes closest to removing the differences between measured and predicted cross sections. Here the amplitude for the $(\alpha,{}^3\mathrm{He};{}^3\mathrm{He},d)$ channel was increased arbitrarily by a factor of 3.0. (Such an increase comes about, approximately, if the ^{3}He distorting potential in the two-step calculation is made equal to the triton potential.) With this boost the $(\alpha,t;t,d)$ and $(\alpha,{}^3\mathrm{He};{}^3\mathrm{He},d)$ contributions become comparable and the interference with the one-step transfer becomes as pronounced as suggested by experimental cross sections.

A comparison of the measured and calculated integrated cross sections is given in Fig. 18 for all states of the ground-state multiplet and two additional high-spin states which in ^{210}Bi have rather pure configurations. The solid horizontal bars give the (absolute) cross sections obtained by using the predetermined two-step normalizations of Sec. V D. The dashed bars are obtained similarly, but the $(\alpha,{}^3\mathrm{He};{}^3\mathrm{He},d)$ amplitude, the weakest of the set, was multiplied by 3.0 so as to become comparable to the $(\alpha,t;t,d)$ amplitude. The improvement over the one-step analysis (Fig. 10) is substantial, even in the unmodified case.

The 9^-, 8^-, 10^-, 11^+, 12^+, and 14^- J_{max} states

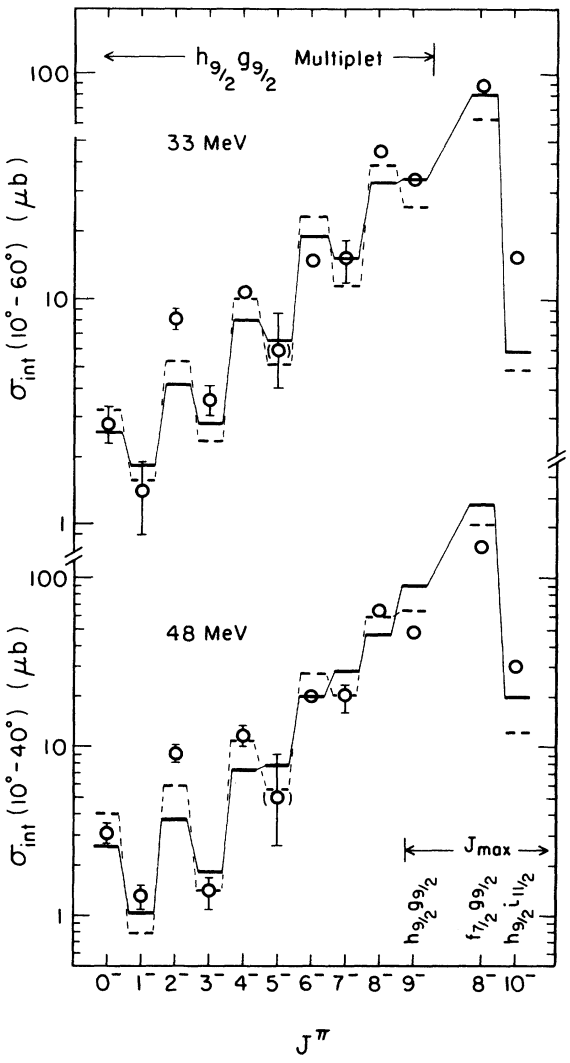

FIG. 18. Comparison of integrated experimental ^{208}Pb (α, d) cross sections for 33 and 48 MeV with second-order-DWBA calculations incorporating direct and sequential stripping amplitudes. Experimental cross sections are shown as circles with error bars where uncertainties exceed the size of the circles. The calculated cross sections are shown as short horizontal bars. The connecting (sloping) lines are drawn to guide the eye. The solid lines connect the calculations with no adjustable parameters. The dashed lines refer to calculations where the $(\alpha, {}^3\mathrm{He}; {}^3\mathrm{He}, d)$ transition amplitude has been arbitrarily scaled up by a factor of 3 to make it comparable to the $(\alpha, t; t, d)$ transition, all else being kept unchanged. We remind the reader that the one-step DWBA prediction corresponds to a smoothly rising line (see Ref. 14) constituting a rough average of the $(h_{9/2}g_{9/2})$ data points, and rising like the data by a factor of 25 at 33 MeV and by a factor of 68 at 48 MeV as J^{π} increases from 0^- to 9^-. All J_{max} states analyzed have second-order DWBA cross sections which lie below the one-step DWBA values.

listed in Sec. IV were found at energies close to those calculated in Ref. 26 and have predicted purities of $\geq 97\%$. The lowest three of these (9^-, 8^-, 10^-) are included in Fig. 18 and are well known, while the three higher lying ones have only tentative assignments. The results of second-order DWBA calculations obtained for these states with the wave functions of Ref. 26 are also in reasonable agreement with experiment. In all six cases the sequential stripping contributions interfere destructively with the one-step amplitude and reduce the predicted cross sections by 14–44%. A comparison with Fig. 10 shows that this change would lead to better agreement with experiment for all J_{max} states but the 10^- and 14^- states. However, the comparison of integrated cross sections may not be very meaningful in view of the marginal agreement seen in the angular distributions for large L. As noted above, the ability of our DWBA curves to match observed cross sections at forward angles decreases systematically with L for $L > 7$. It was seen in Fig. 7 that this situation was only slightly improved for finite range calculations. It is possible that current DWBA procedures may be inadequate for the large momentum mismatch encountered here.

The inclusion of sequential stripping in our calculations leads to improvements in the integrated cross sections, but it does not simultaneously produce better agreement between measured and calculated angular distributions for large L transfer. The analysis of the high spin states seems to throw more light on limitations of DWBA at high L transfer than on the success of our sequential transfer calculations. It is perhaps useful to recall that (α, d) angular distributions to J_{max} states historically have been difficult to fit.

VI. SUMMARY AND DISCUSSION

The ^{208}Pb(α, d) reaction was found to excite many previously known and unknown levels in ^{210}Bi. At 33 MeV the angular distributions are flat and show little structure. At 48 MeV the reaction yields strongly forward peaked cross sections, as low as 2 μb/sr for the ^{210}Bi ground state (1^-) and as high as 300 μb/sr for the prominent 11^+ state at 1.316 MeV (see Fig. 2). Due to the large solid angle and high resolving power of QDDD spectrographs, angular distributions for weak as well as strong states could be extracted with reasonable accuracy. As seen in Figs. 3–7 they show a moderate but consistent structure indicative of the L transfer. One-step microscopic DWBA calculations account for the trend but not the

details of the observed transition strengths; i.e., they match the known final states only to within scale factors of about 0.5–3.0 (Fig. 10). The largest disagreements tend to come from states excited by small L transfer, but discrepancies by factors of up to 2.7 are also seen for the very strong high-spin states.

The modification of the direct one-step amplitude—*whether strong or weak*—by sequential stripping amplitudes is significant in all cases investigated. Cross-section modification by factors of 0.5 to 2 were typical for transitions to the $(h_{9/2}g_{9/2})$ multiplet; factors of 0.5 to 0.8 were typical for the J_{max} states. Experimentally and theoretically the pure $(h_{9/2}g_{9/2})$ ground-state multiplet proved particularly interesting because the observed and computed decrease or increase of the one-step predictions alternated systematically as J_{final} changed from odd to even. The inclusion of the main sequential transfer channels reproduced this effect (Fig. 18). It is noted that the J transfers enhanced or decreased by sequential stripping terms depend on the configuration; e.g., in the $(f_{7/2}g_{9/2})$ multiplet the natural parity states are enhanced and the unnatural ones are weakened. In the present calculation with parameters determined by the observed single-nucleon transfers, the major part of the (α,d) cross-section modification comes from the $(\alpha,t;t,d)$ amplitude. We pointed out, however, that if the $(\alpha,{}^3\mathrm{He};{}^3\mathrm{He},d)$ channel would show less suppression relative to $(\alpha,t;t,d)$ (it now amounts to a factor 3.0 in the amplitude), its effect would be very important in closing the gap remaining between the data and calculations.

We were not able to find a 58 MeV α potential which simultaneously produced *good* fits to elastic scattering *and* to all (α,t) and (α,d) reactions. Potentials with an unconventional shape or a full finite-range or CRC treatment including the nonorthogonality terms may prove necessary for agreement in detail. The sequential-stripping components in our zero-range calculations produce only minor changes in the angular distributions unless cancellations are severe. The failure to fit the small-angle cross sections for large L values seems to present a particularly difficult problem. Generally, DWBA has been found to work best if the momentum transfer is small relative to the momentum of the incident projectile. This is certainly not the case in the $\mathrm{Pb}(\alpha,d)$ reaction. On the other hand, a very similar momentum mismatch existed for one earlier $\mathrm{Pb}(d,\alpha)$ work,[3,50] but showed less pronounced consequences. It may be pertinent that the L transfers of concern here are unusually large. Transitions with $L=13$ have rarely been seen in a direct transfer reaction, nor is their analysis in DWBA terms well understood.

In Fig. 8 we summarize the comparison between current shell model calculations and the existing experimental information for ^{210}Bi. States strongly populated in the current experiment tend to have $J>5$ and frequently represent "stretched" configurations, i.e., $(j_1j_2)_{J_{max}}$. Particularly the latter can easily be correlated with the shell model calculations, which seem to give a reasonable, but by no means precise, account of the experimental situation. Agreement is best for the $(h_{9/2}g_{9/2})$ multiplet, i.e., below 700 keV excitation. Surprisingly, all predictions for the $(h_{9/2}i_{11/2})_{10^-}$ state at 673 keV are in error by about ± 250 keV. The $(f_{7/2}g_{9/2})_{8^-}$ state is well predicted by Refs. 26 and 27, but not by Ref. 25 where the prediction is about 350 keV too high. Reference 25 also fails to predict the strong 11^+ state. This state appears about 300 keV too high in Ref. 26 and 450 keV too low in Ref. 27. There is a general trend to find the J_{max} states at too low an excitation in Ref. 27 and at too high an excitation in Ref. 26. Generally, the predictions of Ref. 26 (approximation II) show the best agreement with experiment.

A comparison with the previous study[50] of $^{208}\mathrm{Pb}(d,\alpha)^{206}\mathrm{Tl}$, which tested a transfer reaction and shell-model calculations[25,26] for ^{206}Tl that closely correspond to the present situation, seems to suggest fewer and smaller discrepancies for the ^{206}Tl case, particularly with respect to the applicability of one-step DWBA. In the ^{206}Tl study and for most other previously investigated (d,α) reactions, the selection rules and angular distributions derived from the one-step model generally have been well supported by the data, and two-step processes were invoked and thought to be of importance primarily for forbidden or unfavored transitions.[6-11,51,52] Thus the question arises why two-step effects might be more evident in the $^{208}\mathrm{Pb}(\alpha,d)$ reaction. One apparent reason is that the ^{210}Bi wave functions for many states are better known than for the other nuclei previously investigated, and any significant discrepancy between experiment and transfer calculations is ascribed to the assumed reaction mechanism. However, we feel that this may not be the sole reason.

A look at common aspects of other (α,d) and (d,α) reactions that presented unusual difficulties for a microscopic one-step transfer analysis[13,52] may give a clue to a more interesting reason. In Ref. 52 the greatest difficulty was encountered in explaining the (α,d) angular distributions for the 6^+ and 4^+ members of the $(\Pi f_{7/2}\nu f_{7/2}^{-1})$ multiplet of ^{48}Sc. In Ref. 13 (d,α) transitions to the

3^+ to 7^+ members of the rather pure $(\Pi g_{9/2}\nu d_{5/2}^{-1})$ multiplet could not be explained until two-step contributions were included in the calculation. All of these "difficult" transitions lead to unusually pure final states as does the ^{208}Pb(α,d) ^{210}Bi reaction. One might speculate that two-step effects in (α,d) transfer are less visible and perhaps have a less pronounced net effect when the transition goes to states with significant configuration mixing. Such a hypothesis would explain why the ^{208}Pb$(d,\alpha)^{206}$Tl one-step analysis[50] was successful, although target, projectile energies, and momentum mismatch were nearly identical to the present study. (The low-lying states in ^{206}Tl are considerably less pure than in ^{210}Bi. Typically, admixed amplitudes in ^{206}Tl are as large as 0.2 or 0.3, whereas admixtures in ^{210}Bi for comparable states rarely exceed 0.1.)

It would be important to investigate if the coherence of various sequential stripping amplitudes in (α,d) reactions parallels that of the one-step amplitudes as is the case for (p,t) transitions to collective states.[12] If this is not the case, the effect of many comparable sequential-transfer amplitudes may become less important than that of the dominant sequential-stripping term seen in ^{208}Pb(α,d).

Finally, it may be asked how accurate it is to neglect the nonorthogonality term and to use a zero-range approach for computations of the type discussed here. Hashimoto and Kawai have addressed a similar question in their theoretical investigation of successive stripping in (p,t) reactions.[12] They find that in (p,t) reactions: (a) sequential stripping amplitudes are comparable to one-step amplitudes; (b) if evaluated in the finite-range approach, nonorthogonality corrections are typically a factor of 10 smaller than other two-step terms and present only a minor problem; and (c) calculations with a finite-range code yield results very similar to a zero-range computation, although the zero-range approach overestimates the nonorthogonality terms by about a factor of 2. Hashimoto and Kawai also noted that the results of their improved theoretical treatment of two-nucleon transfer remained strongly sensitive to the particular sets of optical model parameters used. In particular, the angular distributions were strongly affected by optical-model-parameter ambiguities. We found that calculations for the (α,d) reaction are similarly sensitive to details of the optical model parametrization. Existing parameter deficiencies tend to retain their full importance after inclusion of the sequential stripping terms.

Recently, it has been shown by Hashimoto[53] that the virtual breakup of the intermediate projectile [the deuteron in the (p,t) case] increases in importance with energy. The effects of such breakup terms on the two-step terms can become quite important at small angles. This raises the possibility that the neglect of the virtual breakup term may contribute to our failure to fit small angles for large L transfer.

Theoretical tests for (α,d) reactions similar to those of Refs. 12 and 53 are outside the scope of this paper; however, it appeared reasonable to proceed with a zero-range analysis on the assumption that results qualitatively similar to those for (p,t) reactions would be found for (α,d) reactions at similar energies. Our results lead us to conclude that great caution must be exercised if the strength of two-particle transfers is computed in order to test calculated nuclear wave functions.

ACKNOWLEDGMENTS

This work has been supported in part by a grant from the National Science Foundation. The 33 MeV measurements were made possible by the Max Planck Institut für Kernphysik, Heidelberg, and we benefited greatly from the help and assistance of H. Hafner, H. H. Duhm, R. Seehars, M. Goldschmidt, and C. A. Wiedner. For the 48 MeV measurements at Princeton we had the valuable help of R. M. DelVecchio and W. Oelert.

[1] I. S. Towner and J. C. Hardy, Adv. Phys. 18, 401 (1969).
[2] E. R. Flynn *et al.*, Phys. Rev. C 3, 2371 (1971).
[3] R. M. DelVecchio and W. W. Daehnick, Phys. Rev. C 6, 2095 (1972); W. W. Daehnick and R. M. DelVecchio, *ibid.* 11, 623 (1975).
[4] B. Bayman, Nucl. Phys. A205, 513 (1973); A168, 1 (1971).
[5] N. Austern, R. M. Drisko, E. Rost, and G. R. Satchler, Phys. Rev. 128, 733 (1962).
[6] T. Tamura, Rev. Mod. Phys. 37, 679 (1965).
[7] J. L. Yntema and G. R. Satchler, Phys. Rev. 161, 1137 (1967).
[8] H. H. Duhm *et al.*, Phys. Lett. 48B, 1 (1974).
[9] N. B. DeTakacsy, Nucl. Phys. A231, 243 (1974).
[10] K. Yagi *et al.*, Phys. Rev. Lett. 40, 161 (1978).
[11] R. J. Ascuitto and N. V. Glendenning, Phys. Rev. C 2, 1260 (1970).
[12] N. Hashimoto and M. Kawai, Phys. Rev. Lett. 59B, 223 (1975); Prog. Theor. Phys. 59, 1245 (1978).
[13] W. R. Coker, T. Udagawa, and J. R. Comfort, Phys. Rev. C 10, 1130 (1974).
[14] W. W. Daehnick, M. J. Spisak, J. R. Comfort, H. Hafner, and H. H. Duhm, Phys. Rev. Lett. 41, 639

(1978).
[15]R. E. A. Renfordt, Diplomarbeit, Max-Planck-Institut für Kernphysik, Heidelberg, 1973 (unpublished).
[16]R. T. Kouzes, Ph.D. thesis, Princeton University, 1974 (unpublished).
[17]W. W. Daehnick, M. J. Spisak, R. M. DelVecchio, and W. Oelert, Phys. Rev. C 15, 594 (1977).
[18]J. R. Comfort, ANL Physics Division Informal Report No. PHY-1970B (unpublished).
[19]Our finite range calculations assumed a cluster transfer and were performed with code LOLA written by R. DeVries (unpublished). Some cross checks were made with code DWUCK5, written by P. D. Kunz, University of Colorado (unpublished).
[20]C. Moazed, K. Nagatani, and A. M. Bernstein, Nucl. Phys. A139, 1 (1969); H. Nann *et al.*, *ibid.* A292, 195 (1977); M. B. Lewis, Phys. Rev. 184, 1081 (1969).
[21]M. J. Schneider and W. W. Daehnick, Phys. Rev. C 4, 1649 (1971).
[22]M. B. Lewis, Nucl. Data Sheets B5, 647 (1971).
[23]T. R. Cañada *et al.*, Nucl. Phys. A205, 145 (1973).
[24]J. J. Kolata and W. W. Daehnick, Phys. Rev. C 5, 568 (1972). See also, C. K. Cline *et al.*, Nucl. Phys. A186, 273 (1972).
[25]Y. E. Kim and J. O. Rasmussen, Phys. Rev. 135, B44 (1964); Nucl. Phys. 61, 173 (1965); 47, 184 (1963).
[26]T. T. S. Kuo and G. H. Herling, Naval Research Laboratory Report No. 2258, 1971 (unpublished). See also, G. H. Herling and T. T. S. Kuo, Nucl. Phys. A181, 113 (1972). We use the wave functions for approximation II.
[27]C. W. Ma and Wm. True, Phys. Rev. C 8, 2313 (1973), and private communication.
[28]N. K. Glendenning, Phys. Rev. 137, B102 (1965).
[29]DWUCK4, written by P. D. Kunz, University of Colorado (unpublished). See also, H. W. Baer *et al.*, Ann. Phys. (N.Y.) 76, 437 (1973). This code uses the method of Bayman and Kallio, Phys. Rev. 156, 1121 (1967) for the construction of the form factors for two-nucleon transfer.
[30]W. W. Daehnick, J. D. Childs, and Z. Vrcelj, Phys. Rev. C 21, 2253 (1980).
[31]F. D. Becchetti and G. W. Greenlees, in *Proceedings of the Third International Symposium on Polarization Phenomena in Nuclear Reactions, Madison, Wisconsin, 1970*, edited by H. H. Barschall and W. Haeberli (University of Wisconsin Press, Madison, Wisconsin, 1971), p. 682.
[32]S. M. Barr and R. M. DelVecchio, Phys. Rev. C 15, 114 (1975).
[33]R. Tickle and W. S. Gray, Nucl. Phys. A247, 187 (1975).
[34]T. Omura, B. Imanishi, M. Ichimura, and M. Kawai, Prog. Theor. Phys. (Kyoto) 44, 1242 (1970).
[35]W. R. Coker, T. Udagawa, and H. H. Wolter, Phys. Rev. C 7, 1154 (1973).
[36]G. R. Satchler, Nucl. Phys. 55, 1 (1964).
[37]B. F. Bayman and A. Kallio, Phys. Rev. 156, 1121 (1967).
[38]Code CHUCK3 is the version of CHUCK2 extended by J. R. Comfort. CHUCK2 was written by P. D. Kunz, University of Colorado (unpublished) and is a zero-range CRC computer program. CHUCK2 was made available to us in two versions dated 1977 and 1979 which differ in their phase conventions. CHUCK3 corresponds to the later version.
[39]J. R. Comfort. Comput. Phys. Commun. 16, 35 (1978).
[40]M. H. Macfarlane and J. B. French, Rev. Mod. Phys. 32, 567 (1960).
[41]J. P. Schiffer in *Isospin in Nuclear Physics*, edited by D. H. Wilkinson (North-Holland, Amsterdam, 1969).
[42]N. Austern, *Direct Nuclear Reaction Theories* (Wiley, New York, 1970).
[43]J. R. Comfort and B. C. Karp, Phys. Rev. C 21, 2162 (1980).
[44]J. R. Comfort and B. C. Karp, Phys. Lett. 80B, 1 (1978).
[45]P. D. Kunz in *The* (p,n) *Reaction and the Nucleon-Nucleon Force*, edited by C. D. Goodman, S. M. Austin, S. D. Bloom, J. Rapaport, and G. R. Satchler (Plenum, New York, 1980).
[46]J. S. Lilley and N. Stein, Phys. Rev. Lett. 19, 709 (1967).
[47]R. J. Bardwick and R. Tickle, Phys. Rev. 171, 1305 (1968).
[48]G. Igo *et al.*, Phys. Rev. 177, 1831 (1969).
[49]D. Kovar, N. Stein, and C. K. Bockelman, Nucl. Phys. A231, 266 (1974).
[50]M. B. Lewis and W. W. Daehnick, Phys. Rev. C 1, 1577 (1970).
[51]W. W. Daehnick and R. Sherr, Phys. Rev. C 7, 150 (1973).
[52]A. Richter *et al.*, Phys. Rev. C 5, 814 (1972).
[53]N. Hashimoto, Prog. Theor. Phys. 63, 853 (1980).